Vol. 2 • No. 3 • March • 2014

www.advopticalmat.de

ADVANCED OPTICAL MATERIALS

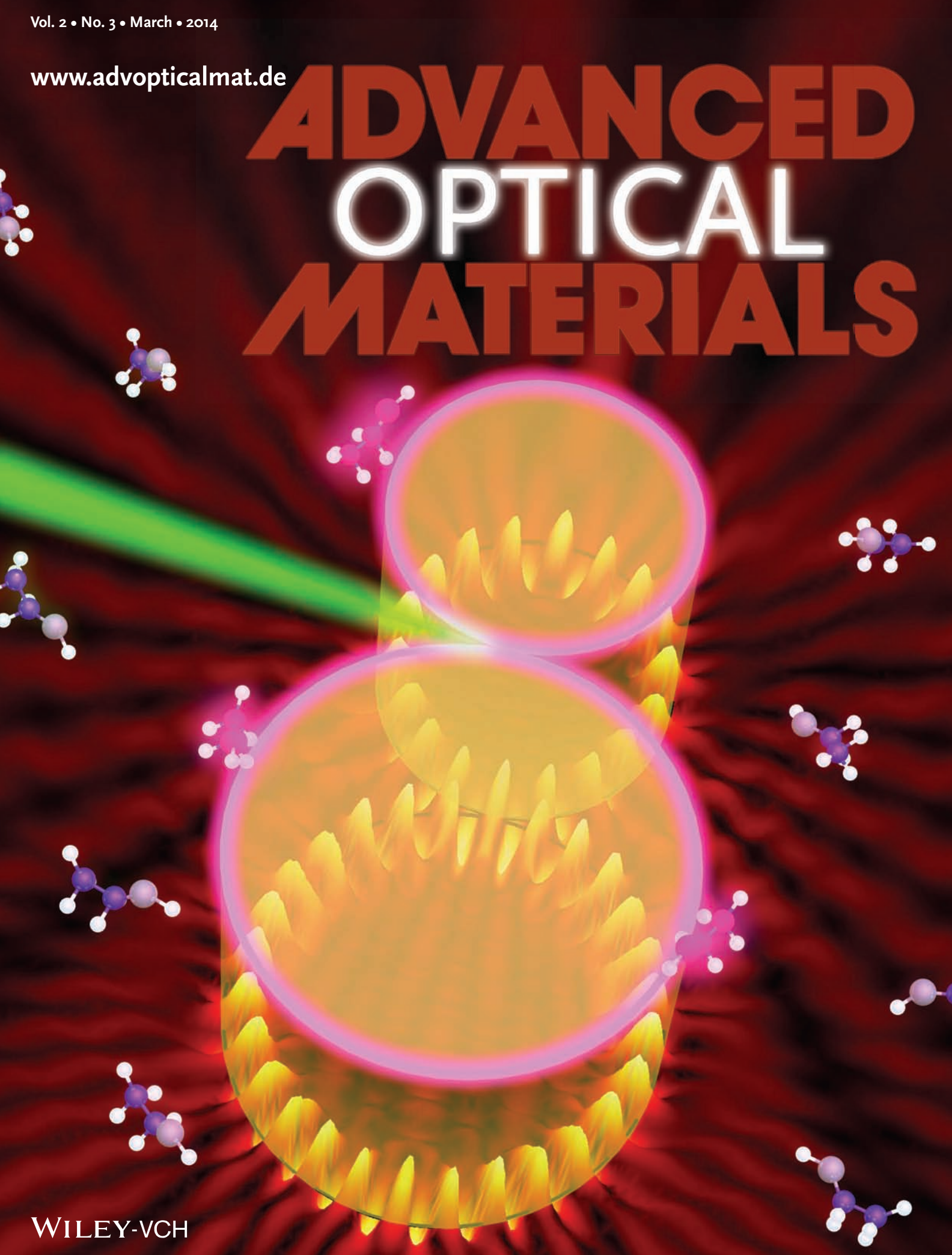

WILEY-VCH

ADVANCED OPTICAL MATERIALS
www.advopticalmat.de

Materials Views
www.MaterialsViews.com

Coupled Polymer Microfiber Lasers for Single Mode Operation and Enhanced Refractive Index Sensing

*Van Duong Ta, Rui Chen, and Handong Sun**

Owing to high quality (*Q*) factor and unique cavity configuration, whispering gallery cavities (WGCs) have attracted intensive research attentions in diverse fields of sciences and technologies such as quantum electrodynamics, optical chaos, optical filters, modulators, and lasers.[1–9] Recently, WGCs have exhibited promising applications as chemical and biological sensors based on the shifting or splitting of resonance modes.[10–14] This technique is label-free and ultra-sensitive down to the level of nanoparticles, viruses, and even single molecules.[12–14] For such sensors, both high *Q* factor and large free spectral range (FSR) are strongly desirable. However, these two factors are normally conflicting in a single cavity.

Recently, investigations on coupled WGCs have demonstrated many interesting phenomena like induced transparency and absorption, slow light,[15,16] directional and single mode emission,[17–22] and enhancement of sensor's sensitivity.[23,24] Single mode lasing is significant for integrated photonics and on-chip applications.[25] Traditionally, it has been realized by configurations including Fabry-Pérot (F-P)[25] and especially distributed feedback (DFB) cavities.[26–28] For WGCs, single mode operation can be obtained by reducing the cavity size,[29] but this method deteriorates laser *Q* factor. The alternative solution without deteriorating the *Q* factor is to use coupled WGCs, in which single mode emission is generated through Vernier effect.[19,20] Coupled WGCs have been explored in microdisks, optofluidic ring resonators, and silica/glass fibers.[17–24]

Compared to traditional semiconductor and inorganic one-dimensional cavities, organic nano/microfibers possess simpler fabrication and better mechanical flexibility, thus are attractive for flexible optoelectronics and nanophotonics.[30,31] They are also easier to be assembled in arrays or ordered structures,[32] highly beneficial for photonic systems, and have successfully employed for logic elements/circuits.[33] However, nano/microfiber lasers, being an important component in integrated photonic devices, have been mostly limited to waveguide effect where two endfaces of the fiber served as reflection mirrors.[32,34–37] Generally, this mechanism has low *Q* factor because of poor reflectivity of the endface reflectors, which hinders it for practical applications, especially in biological sensors. Very recently, we have achieved high *Q* factor whispering gallery mode (WGM) lasing, inside a circular cross-section of a straight polymer fiber, with potential application as a sensitive refractive index sensor.[38] Further investigation of coupled fiber structures should be important not only for improving the laser and sensor performances, but also for exploring a possibility to integrate with other components, which is significant for optical filters, optical circuits.

Herein, we present our successful realization of single mode operation from coupled fibers via the Vernier effect. Furthermore, we have found that this coupling effect offers a solution to the conflicting problem, high sensitivity and large FSR, in optical sensors based on WGM technology. Application of the coupled fiber laser as a refractive index sensor exhibits sensitivity about 400 nm/refractive index unit (RIU) while only 210 nm/RIU for a single one.

In a coupled WGC, resonance modes circulate in each resonator can interact with each other. In the strong interaction case, one cavity can be considered as a spectral filter to the resonance wavelengths of the other one. As a result, certain resonance modes will be enhanced when fulfilling both resonance conditions of the two isolated cavities, while other modes will be depressed, and this phenomenon is known as Vernier effect.[39–41] Suppose the FSR of the first and the second cavities are FSR_1, FSR_2, respectively, then the condition for observing the Vernier effect is $N_1FSR_1 = N_2FSR_2$, where N_1 and N_2 are co-prime integers. Obviously, FSR of the coupled cavity (FSR_{12}) can be calculated as $FSR_{12} = N_1FSR_1 = N_2FSR_2$. This effect artificially increases FSR and has been widely applied for optical filters, optical wavelength division multiplexing systems.[39–42] The increase of FSR is also a key factor for single mode operation, which becomes possible when the FSR exceeds the gain region of active material.[43]

Figure 1 shows the normalized distribution of transverse magnetic (TM) field, simulated using the finite element method (FEM) via COMSOL Multiphysics, in a coupled asymmetric cavity with radii 2.237 and 1.5 μm. The refractive index of both cavities is 1.48 and the distance between them is chosen around 0.05λ for strongly interacting WGMs.[44] Here, λ is the resonance wavelength characterized by mode order *r* and mode number *m*.[45] Figure 1a shows mode distribution in the coupled cavity when both cavities are on resonance at $\lambda = 630$ nm corresponding to (r, m) = (1, 28) and (1, 18) for the big and small cavity, respectively. As expected, the coupled cavity is on resonance verified by the presence of resonance patterns. The overlap of maximum field positions in both cavities is clearly seen at the coupling region. However, when only the big cavity is on resonance at $\lambda = 651.3$ nm equivalent to (r, m) = (1, 27), the field in the coupled structure is highly diverged and the

V. D. Ta, Dr. R. Chen, Prof. H. D. Sun
Division of Physics and Applied Physics
School of Physical and Mathematical Sciences
Nanyang Technological University
Singapore, 637371, Singapore
E-mail: hdsun@ntu.edu.sg
Prof. H. D. Sun
Centre for Disruptive Photonic Technologies (CDPT)
Nanyang Technological University
Singapore, 637371, Singapore

DOI: 10.1002/adom.201300433

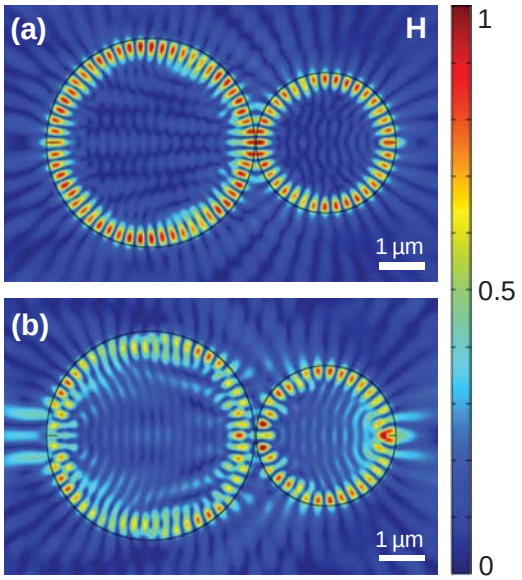

Figure 1. Normalized magnetic field distribution inside a coupled cylindrical cavity when (a) both cavities are on resonance and (b) only the big cavity is on resonance.

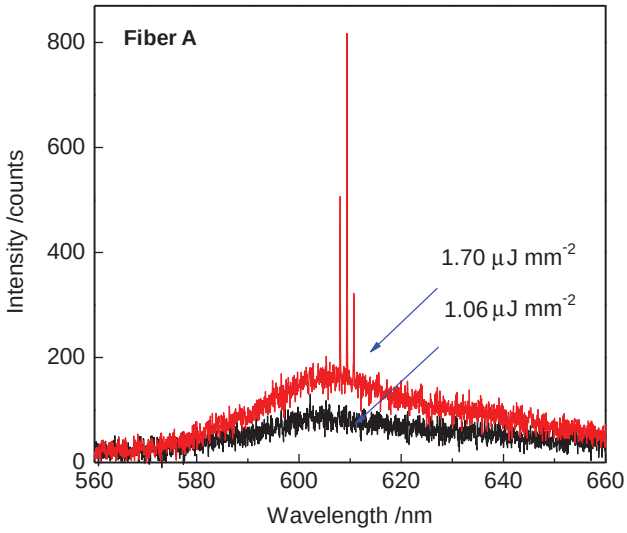

Figure 3. The PL spectra from a fiber A, below and just above lasing threshold.

mode intensity is relatively weak (Figure 1b), implying the suppression of this mode. Similar results can be obtained for other modes existing in the two isolated cavities. These numerical simulations validate the feasibility of achieving single longitudinal mode lasing through the Vernier effect.

Based on the above idea, polymer fibers with suitable sizes (there should be certain lasing modes that fulfilled the resonance condition of both cavities) are chosen to demonstrate the Vernier effect. The investigated structure is schematically shown in **Figure 2**. Isolated and coupled fibers are placed on a distributed Bragg reflector (DBR) substrate and studied subsequently. The DBR is important for reducing the lasing threshold because it prevents optical leakage though the substrate.[7] The stop band of the DBR (from around 575 to 720 nm) covers the emission range of the gain material with a reflectivity up to 99% at 640 nm. The coupled fiber is achieved by direct contacting the two isolated fibers and then fixed on the DBR by two drops of glue (PMMA solution) (Figure 2b). The same optical characterization processes (see Experimental Section) were performed on the two isolated and the coupled fibers to facilitate the comparison of the lasing properties.

FSR is a key parameter for studying the Vernier effect. Given that WGMs are generated inside circular cross-sections of fibers (Figure 2), FSR of fibers with diameters D_1 and D_2 can be approximately calculated as follows:

$$\mathrm{FSR}_{1(2)} = \frac{\lambda^2}{\pi n_{\mathrm{eff}} D_{1(2)}} \quad (1)$$

where n_{eff} is effective refractive index of the fibers. FSR of the coupled cavity (FSR_{12}), however, efficiently increases and can be estimated by Vernier equation ($D_2 > D_1$):[20]

$$\mathrm{FSR}_{12} = \frac{\lambda^2}{\pi n_{\mathrm{eff}} (D_2 - D_1)} \quad (2)$$

Figure 3 plots the photoluminescence (PL) spectra from a fiber (fiber A) at pump fluence of 1.06 and 1.70 μJ mm^{-2}. At the low excitation density, the fiber exhibits broad spontaneous emission (SE) with weak intensity. However, at higher pumping energy, sharp and intense peaks have appeared, indicating a revolution from SE to stimulated lasing emission.

Figure 4 plots the transformation from multi mode lasing of two isolated fibers to single mode emission of a coupled one (denoted as coupled fiber AB). Figures 4a and b show the lasing spectra from the fiber A and the fiber B, respectively, under a pump fluence of about 2.12 μJ mm^{-2}. FSRs of the fiber A and the fiber B are 1.4 and 2.2 nm, respectively. Considering that $\lambda_A = \lambda_B = 608$ nm, $n_{\mathrm{eff}} = 1.48$, and $D_A = 54.5$ μm, $D_B = 35.5$ μm (close to values estimated from optical images), theoretical prediction FSR_A and FSR_B based on the Equation (1) are 1.46 and 2.24 nm, respectively. These FSRs are

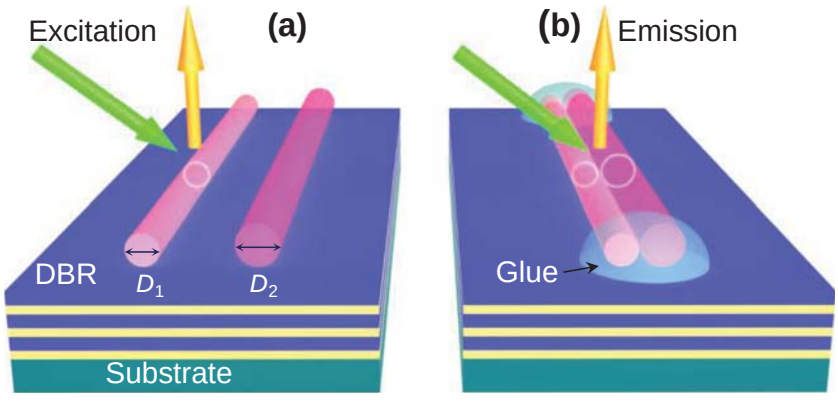

Figure 2. Schematic diagram for optical investigation of Vernier effect. Two asymmetric fibers are (a) isolated and (b) coupled. The white rings inside fibers indicate WGMs.

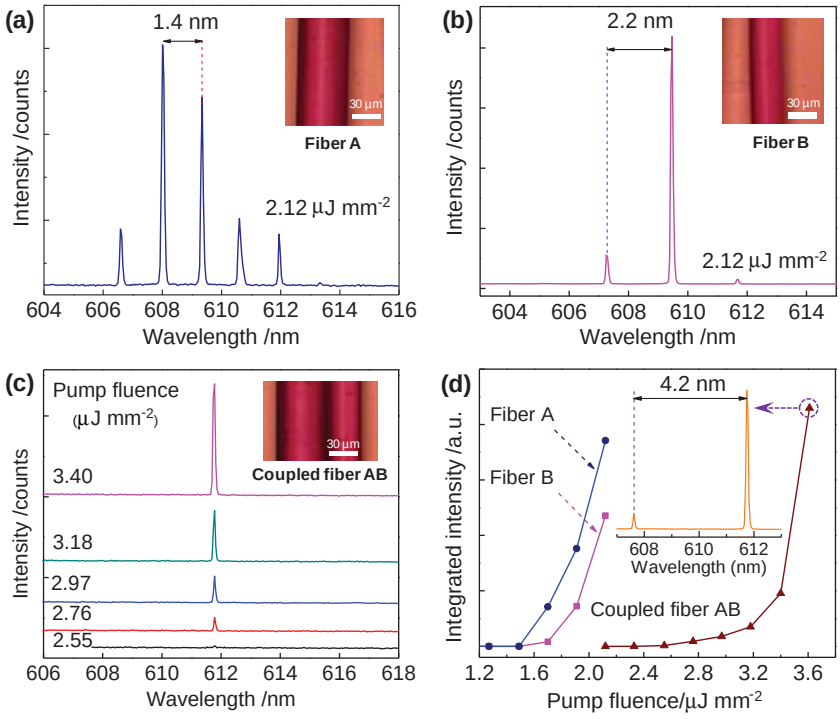

Figure 4. (a,b) Lasing spectra from the fiber A and fiber B at pumping fluence of 2.12 μJ mm^{-2}, respectively. (c) Lasing spectra of a coupled fiber A and fiber B (the so-called coupled fiber AB) under increasing pump energy. Curves are shifted vertically for clarity. Optical images of presented fibers are shown in the insets. (d) Integrated lasing intensity of the fiber A, the fiber B, and the coupled fiber AB as function of pumping fluence. The inset indicates FSR of the coupled fiber AB at pumping fluence of 3.61 μJ mm^{-2}.

consistent with the experiments and therefore verified the WGM mechanism.

Emissions from the coupled fiber AB under different pumping intensities are plotted in Figure 4c. The single mode emission starts to appear at pump fluence of 2.55 μJ mm^{-2}. This mode is maintained with higher intensity at increasing excitation energy (up to 3.40 μJ mm^{-2}), indicating a high efficient suppression of lasing modes.[22] Furthermore, this single mode is not an accident but due to the Vernier effect, which will be elaborated later. For lasing threshold, integrated lasing intensity of the fiber A, fiber B, and coupled fiber AB are shown in Figure 4d. The lasing threshold of the coupled fiber is about 2.6 μJ mm^{-2} and both isolated fibers have almost the same lasing threshold of around 1.6 μJ mm^{-2}. The nearly equal threshold of the isolated fibers is vital for the coupling effect because both fibers are on resonance simultaneously, optical loss is very low and the coupling effect can be easily achieved.[20] In contrast, if the lasing thresholds are much different, one fiber is on resonance while the other is not, the light travels in the coupled cavity will suffer high optical loss, which strongly affects the coupling performance.

Earlier report on a coupled optofluidic ring resonator has shown that the coupling related loss can be very low[19] so there is no clear degradation of lasing Q factor. Similar result was observed in our work, spectral linewidth of lasing mode of the coupled fiber is almost the same compared with the single fibers, which are about 0.09 nm. Obviously, the coupling effect provides single mode operation but does not affect Q factor of individual fibers. This is advantageous compared with single mode operation of single fiber obtained by reducing cavity size.

As mentioned earlier, the single mode emission from the coupled fiber AB is due to the Vernier effect, verified by (i) examining the resonance condition, (ii) position of lasing modes and (iii) comparing the FSR of coupled fiber AB with the single fiber A and fiber B. The resonance condition is fulfilled because FSR_A and FSR_B are 1.4 and 2.2 nm respectively, thus $3FSR_A \approx 2FSR_B$. The single mode from the coupled fiber AB is generated at around 612 nm closed to lasing wavelengths of the both fiber A and fiber B. FSR of the coupled fiber AB (FSR_{AB}) largely increases. The inset of Figure 4d shows the development of second Vernier mode (around 607.6 nm) at pump fluence of 3.61 μJ mm^{-2}, FSR_{AB} is determined to be 4.2 nm. As a result, $FSR_{AB} = 3FSR_A \approx 2FSR_B$. In addition, the spectral separation predicted by using the Equation (2) is 4.18 nm, consistent with experimental data.

The coupling effect is highly repeatable. We studied various other coupled cavities and consistent results are obtained. **Figure 5**a plots multi mode lasing of a fiber namely fiber D with FSR_D = 1.5 nm. This mode spacing effectively increases to 4.4 nm when the fiber D is coupled with a smaller fiber namely fiber C (FSR_C = 2.3 nm, not shown here) to form the so call coupled fiber CD (Figure 5b). In addition, number of lasing mode of the coupled fiber CD is two (single mode was observed at higher pump energy), which is much less than that of the fiber D (seven modes). FSR_{CD} is 4.4 nm, is almost equal to triple FSR_D and double FSR_C. Furthermore, considering that D_C = 36 μm, D_D = 55 μm, $\lambda_C = \lambda_D$ = 640 nm, the prediction of FSR_{CD} using

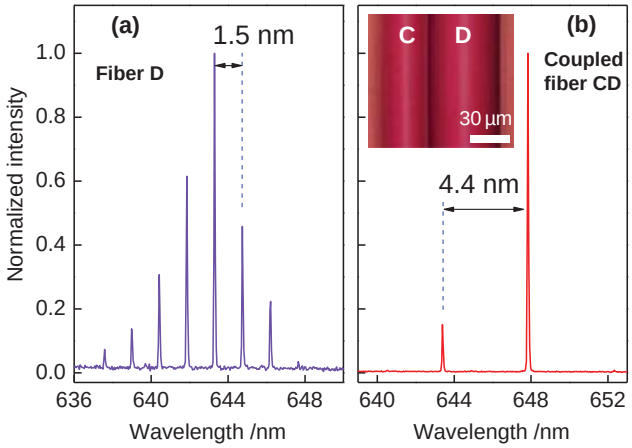

Figure 5. Lasing spectra from (a) a single fiber namely fiber D and (b) a coupled fiber CD. The inset shows optical image of the coupled fiber CD.

Table 1. FSR comparison between experimental observation and calculation of coupled fibers. The calculation is based on the Equation (2).

Diameter of fibers [μm]		FSR of coupled fibers [nm]	
D_1	D_2	Calculation	Experimental
35.5	54.5	4.2	4.2
36.0	55.0	4.6	4.4
24.1	38.1	5.7	5.5

the Equation (2) is to be around 4.6 nm, close to the observation. **Table 1** summarizes FSR of coupled cavities from experimental and calculation for different fibers. The agreement between the observation and prediction concludes that Vernier effect is the key factor on the increase of FSR and the single mode operation.

Figure 6a shows a schematic setup for sensing characterization. The setup is the same as earlier measurements excluding two new channels connected with a beaker. The input channel is for loading a certain volume of ethanol to modify the water medium. However, the adding of ethanol will lift the solution level and affects the transmission of excitation light. Because of that, the coupled fiber is out of focus of excitation beam. In order to prevent this problem, amount of liquid nearly equal to ethanol addition is subtracted through the output channel. The volume of water was 20 mL. Ethanol addition after each measurement was 0.1 mL. Excitation energy was fixed during measurement. The coupled fiber was only excited for a short time (about 1 s) for spectrum recording to avoid degradation of dye molecules. In addition, measurements were carried out after around 40 s from the time when ethanol was added, to make sure that ethanol was fully dissolved in water.

Ethanol molecules diffuse quickly after loading into water. During this process, numerous of ethanol molecules will be trapped on the fiber surface. This number increases as function of time. At the end, it reaches a maximum and almost unchanged. Consequently, a thin layer of ethanol molecules with thickness ΔR is formed covering the fiber surface, schematically indicated in Figure 6b. This layer is a major factor expanding the optical pass of WGMs inside the fiber and leads to red-shift of lasing mode (Figure 6c).[10] Another factor is the increase of refractive index of the solution (Δn). In our work, maximum of Δn is 7.1×10^{-4} RIU. It is equivalent to very small effective index change ($\Delta n_{eff} \sim 10^{-7}$ RIU) inside the fiber so has very weak effect on the spectrum shift. Therefore, resonance shift ($\Delta\lambda$) can be considered as a main product of the thin layer and is estimated as following equation:[10] $\Delta\lambda/\lambda = \Delta R/R$, where R is radius of fiber. It is important to note that even though our sensors respond to the thin layer, it can be surely applied as refractive index sensors. The reason is that the thickness of the thin layer is a function of ethanol concentration. In addition, the refractive index of the ethanol solution changes linearly with its concentration. Therefore, the refractive index sensor can work by establishing the resonance shift $\Delta\lambda$ as a function of refractive index variation (via concentration).

The convenience and improvement of coupled cavity over single cavity as a refractive index sensor are demonstrated. **Figure 7**a and b plot spectra from the coupled fiber CD and a single fiber E ($D_E \sim 47$ μm) as function of ethanol concentration (C_E) from 0 to 1.18 wt%, equivalent to refractive increase Δn from 0 to 7.1×10^{-4} RIU. Lasing mode from the coupled fiber exhibits a larger red-shift compared with that from the single one. Furthermore, have a close look at the case of the coupled fiber, we can see that beside the single mode at around 641 nm, another Vernier mode starts to appear at 645.4 nm when C_E reaches to 0.79 wt%. Likely, this observation is due to the increase of refractive index of liquid solution or decrease of index contrast between the fiber and outside medium. Thus, the emission is less confined and the second Vernier mode can be easier coupling out by scattering and to be observed. Measured FSR of the coupled fiber is still 4.4 nm. It confirms the presence of the Vernier effect in the coupled fiber during the sensing process. For better view, close-up image of main modes from the coupled fiber CD and fiber E are shown in Figure 7c and d, respectively. For the same refractive increase of 7.1×10^{-4} RIU, resonance shift of the coupled fiber CD and the single fiber E are 0.28 and 0.15 nm, respectively. Figure 7e indicates a linear relationship between the resonance shift and refractive index variation, validating the sensing mechanism. Sensitivity of coupled fiber CD and fiber E are 398 and 210 nm/RIU, respectively. Supposing enhancement

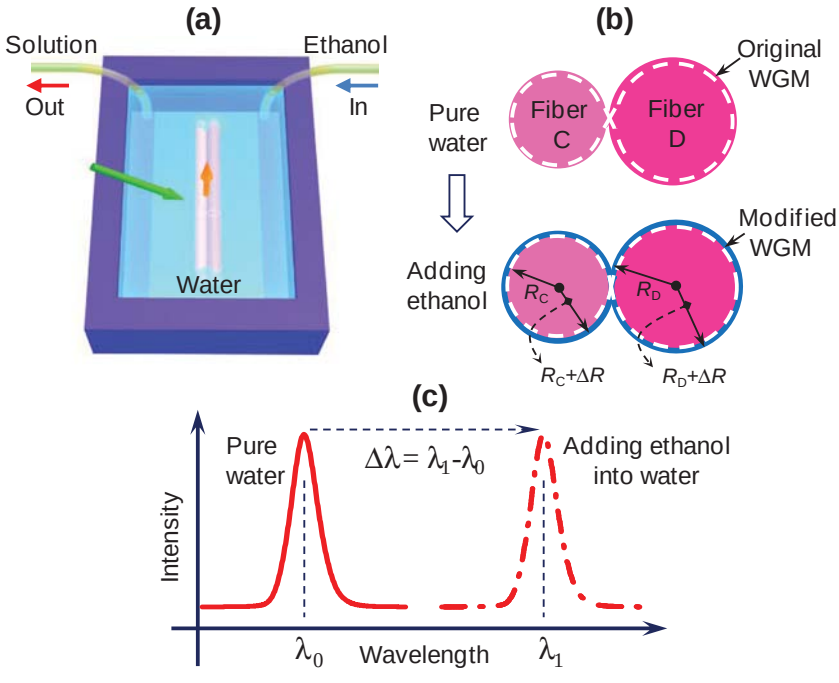

Figure 6. Refractive index sensing application using the coupled fiber CD. (a) Schematic measurement setup, (b) WGM modification before and after the addition of ethanol. The presence of ethanol creates a thin layer of thickness ΔR covering surface of the coupled fiber. (c) Resonance shift ($\Delta\lambda$) of lasing mode is an indicator of the sensor.

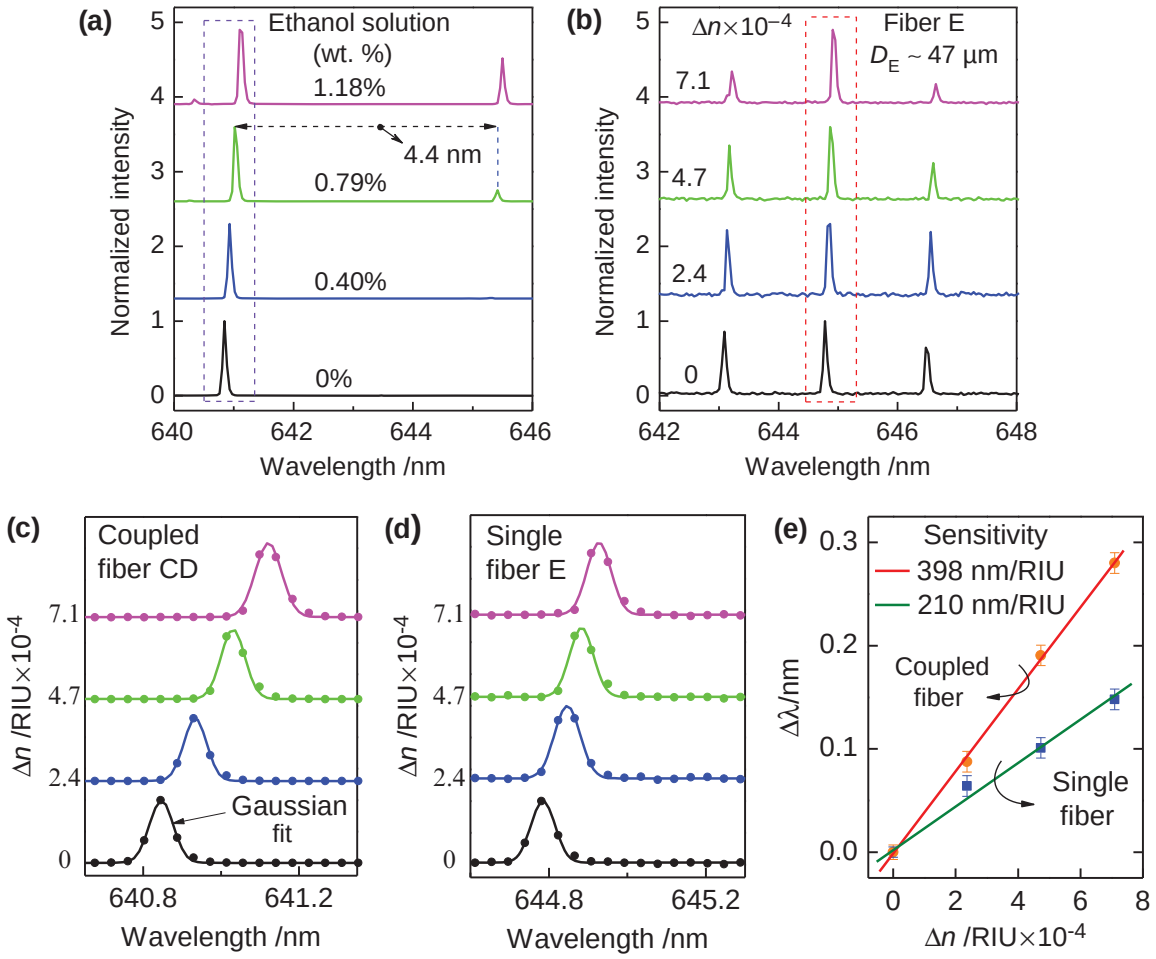

Figure 7. Lasing spectra of (a) the coupled fiber CD and (b) a single fiber namely fiber E under the same condition, posses increasing ethanol concentration or refractive index. (c), (d) Close-up spectra in the dash rectangles of (a) and (b), respectively. Curves are shifted vertically for clarity. (e) Resonance shift of the coupled fiber and single fiber with refractive index change.

factor is a ratio between the sensitivity of coupled fiber CD and single fiber E then experimental enhancement factor is 1.9.

The enhanced sensitivity of coupled cavity over single cavity can be explained by the thin layer theory. Consider earlier assumption, resonance shift of the coupled fiber CD ($\Delta\lambda_{CD}$) and fiber E ($\Delta\lambda_E$) can be estimated as following: $\Delta\lambda_{CD}/\lambda = \Delta R/R_C + \Delta R/R_D$ and $\Delta\lambda_E/\lambda = \Delta R/R_E$ where R_C, R_D, R_E are radii of the fiber C, fiber D, fiber E, respectively. Theoretical enhancement factor is $\Delta\lambda_{CD}/\Delta\lambda_E = (R_C + R_D)R_E/R_CR_D = 2.1$, close to the observation.

We have demonstrated the robust single mode lasing with spectral linewidth as narrow as 0.09 nm from coupled polymer fiber lasers via the Vernier effect. Our achievement indicates the possibility of integrating between polymer fibers, which is a first step to realize all polymer fiber optical switches and optical filters.[46] Interestingly, we have found that using such kind of coupled cavities as WGM optical sensors will solve the conflicting problem between two desired factors, high Q factor and large FSR. Experimental results show coupled structure has higher sensitivity (nearly double in our work) compared with that of single one. We believe the sensitivity of individual cavities both contributes to the sensitivity of the coupled one. Owing to cost effective mass production, high coupling efficiency, single mode lasing emission and high sensor's sensitivity, our work boosts polymer fibers as very competitive candidates for photonic technology, especially flexible optoelectronic devices.

Experimental Section

Polymer Fiber Fabrication: The fibers were fabricated by directly drawn from a solution that has been described in our previous work.[38] The host material of the fiber is a mixture of poly(methyl methacrylate) (PMMA) and Araldite 506 epoxy resin. The gain material is a Rhodamine B (RhB). We dissolved PMMA (100 mg) in dichloromethane (around 1 mL, ~1.28 g), purity 99.76%, to get a 7.3 wt% PMMA solution. Then, epoxy resin (150 mg) and RhB (4 mg), 95% dye content, were added. The dye concentration in the final solution was 0.26 wt%. After fabrication, the fibers were subsequently dried in the air at room temperature for 2–3 days for structure solidification. All chemicals are from Sigma-Aldrich.

Optical Characteristics: The fibers was pumped by a green pulse laser (wavelength: 532 nm, pulse duration: 1 ns, repetition rate: 60 Hz). The excitation spot has an ellipse shape about 0.3 mm × 0.4 mm. The emission from the fiber was collected from the top and recoding by a

silicon charged coupled device (CCD). To avoid high order modes, undesired for characterization of the Vernier effect, all fibers were immersed in water during the measurement.

Acknowledgements

This work is supported by the Singapore Ministry of Education through the Academic Research Fund under Projects MOE 2011-T3-1-005 (Tier 3) and RG63/10 (Tier 1) and from the Singapore National Research Foundation through the Competitive Research Programme (CRP) under Projects No. NRF-CRP6-2010-02 and NRF-CRP5-2009-04).

Received: October 19, 2013
Revised: November 19, 2013
Published online: December 4, 2013

[1] P. Rabiei, W. H. Steier, C. Zhang, L. R. Dalton, *J. Lightwave Technol.* **2002**, *20*, 1968.
[2] K. J. Vahala, *Nature* **2003**, *424*, 839.
[3] V. S. Ilchenko, A. B. Matsko, *IEEE J. Sel. Top. Quantum Electron.* **2006**, *12*, 15.
[4] R. Chen, B. Ling, X. W. Sun, H. D. Sun, *Adv. Mater.* **2011**, *23*, 2199.
[5] J. Ward, O. Benson, *Laser Photon. Rev.* **2011**, *5*, 553.
[6] V. D. Ta, R. Chen, H. D. Sun, *Adv. Mater.* **2012**, *24*, OP60.
[7] R. Chen, V. D. Ta, H. D. Sun, *Sci. Rep.* **2012**, *2*, 244.
[8] Q. J. Wang, C. Yan, N. Yu, J. Unterhinninghofen, J. Wiersig, C. Pflügl, L. Diehl, T. Edamura, M. Yamanishi, H. Kan, F. Capasso, *Proc. Natl. Acad. Sci. USA* **2010**, *107*, 22407.
[9] M. Humar, M. Ravnik, S. Pajk, I. Muševi , *Nature Photon.* **2009**, *3*, 595.
[10] F. Vollmer, S. Arnold, *Nat. Methods* **2008**, *5*, 591.
[11] V. D. Ta, R. Chen, D. M. Nguyen, H. D. Sun, *Appl. Phys. Lett.* **2013**, *102*, 031107.
[12] A. M. Armani, R. P. Kulkarni, S. E. Fraser, R. C. Flagan, K. J. Vahala, *Science* **2007**, *317*, 783.
[13] J. Zhu, S. K. Ozdemir, Y.-F. Xiao, L. Li, L. He, D.-R. Chen, L. Yang, *Nature Photon.* **2010**, *4*, 46.
[14] L. He, S. K. Ozdemir, J. Zhu, W. Kim, L. Yang, *Nature Nanotechnol.* **2011**, *6*, 428.
[15] A. Naweed, G. Farca, S. I. Shopova, A. T. Rosenberger, *Phys. Rev. A* **2005**, *71*.
[16] K. Totsuka, N. Kobayashi, M. Tomita, *Phys. Rev. Lett.* **2007**, *98*, 213904.
[17] Y. Xiao, C. Meng, X. Wu, L. Tong, *Appl. Phys. Lett.* **2011**, *99*, 023109.
[18] H. Li, J. Li, L. Qiang, Y. Zhang, S. Hao, *Nanoscale* **2013**, *5*, 6297.
[19] W. Lee, H. Li, J. D. Suter, K. Reddy, Y. Sun, X. Fan, *Appl. Phys. Lett.* **2011**, *98*, 061103.
[20] L. Shang, L. Liu, L. Xu, *Opt. Lett.* **2008**, *33*, 1150.
[21] Y. Xiao, C. Meng, P. Wang, Y. Ye, H. Yu, S. Wang, F. Gu, L. Dai, L. Tong, *Nano Lett.* **2011**, *11*, 1122.
[22] T. Grossmann, T. Wienhold, U. Bog, T. Beck, C. Friedmann, H. Kalt, T. Mappes, *Light: Sci. Appl.* **2013**, *2*, e82.
[23] S. I. Shopova, Y. Sun, A. T. Rosenberger, X. D. Fan, *Microfluid. Nanofluid.* **2009**, *6*, 425.
[24] H. Li, L. Shang, X. Tu, L. Liu, L. Xu, *J. Am. Chem. Soc.* **2009**, *131*, 16612.
[25] G. Aubry, Q. Kou, J. Soto-Velasco, C. Wang, S. Meance, J. J. He, A. M. Haghiri-Gosnet, *Appl. Phys. Lett.* **2011**, *98*, 111111.
[26] Z. Li, Z. Zhang, T. Emery, A. Scherer, D. Psaltis, *Opt. Express* **2006**, *14*, 696.
[27] M. Gersborg-Hansen, A. Kristensen, *Opt. Express* **2007**, *15*, 137.
[28] F. Todescato, I. Fortunati, S. Gardin, E. Garbin, E. Collini, R. Bozio, J. J. Jasieniak, G. Della Giustina, S. Toffanin, R. Signorini, *Adv. Funct. Mater.* **2012**, *22*, 337.
[29] V. D. Ta, R. Chen, H. D. Sun, *Sci. Rep.* **2013**, *3*, 1362.
[30] D. Li, Y. Xia, *Adv. Mater.* **2004**, *16*, 1151.
[31] A. Camposeo, L. Persano, D. Pisignano, *Macromol. Mater. Eng.* **2013**, *298*, 487.
[32] A. Camposeo, F. Di Benedetto, R. Stabile, A. A. R. Neves, R. Cingolani, D. Pisignano, *Small* **2009**, *5*, 562.
[33] M. Hamedi, R. Forchheimer, O. Inganas, *Nature Mater.* **2007**, *6*, 357.
[34] D. O'Carroll, I. Lieberwirth, G. Redmond, *Nature Nanotechnol.* **2007**, *2*, 180.
[35] Y. S. Zhao, A. Peng, H. Fu, Y. Ma, J. Yao, *Adv. Mater.* **2008**, *20*, 1661.
[36] A. J. Das, C. Lafargue, M. Lebental, J. Zyss, K. S. Narayan, *Appl. Phys. Lett.* **2011**, *99*, 263303.
[37] C. Zhang, C.-L. Zou, Y. Yan, R. Hao, F.-W. Sun, Z.-F. Han, Y. S. Zhao, J. Yao, *J. Am. Chem. Soc.* **2011**, *133*, 7276.
[38] V. D. Ta, R. Chen, L. Ma, Y. J. Ying, H. D. Sun, *Laser Photon. Rev.* **2013**, *7*, 133.
[39] K. Oda, N. Takato, H. Toba, *J. Lightwave Technol.* **1991**, *9*, 728.
[40] G. Griffel, *IEEE Photonics Technol. Lett.* **2000**, *12*, 1642.
[41] P. Urquhart, *J. Opt. Soc. Am. A* **1988**, *5*, 803.
[42] R. Orta, P. Savi, R. Tascone, D. Trinchero, *IEEE Photonics Technol. Lett.* **1995**, *7*, 1447.
[43] J. Schäfer, J. P. Mondia, R. Sharma, Z. H. Lu, A. S. Susha, A. L. Rogach, L. J. Wang, *Nano Lett.* **2008**, *8*, 1709.
[44] J.-W. Ryu, S.-Y. Lee, C.-M. Kim, Y.-J. Park, *Phys. Rev. A* **2006**, *74*, 013804.
[45] C. C. Lam, P. T. Leung, K. Young, *J. Opt. Soc. Am. B* **1992**, *9*, 1585.
[46] X. Jiang, Y. Chen, G. Vienne, L. Tong, *Opt. Lett.* **2007**, *32*, 1710.